High energy photon production in nuclear collisions

K. Nakayama and G. Bertsch
Department of Physics and Astronomy and Cyclotron Laboratory, Michigan State University, East Lansing, Michigan 48824
(Received 2 June 1986)

High energy photons may be produced in nuclear reactions by several mechanisms, including bremsstrahlung from the potential field or from nucleon-nucleon collisions. Using infinite and semi-infinite nuclear matter approximations, we obtain simple expressions for the rates. Nucleon-nucleon collisions provide the more important mechanism for both proton-induced and heavy-ion induced reactions, except for the highest energy photons. The photon cross section calculated with a zero range np interaction agrees well with measurements on proton-induced reactions. For heavy-ion reactions, the initial np collisions only account for a third of the measured cross section. The disagreement may be due to an inadequacy of the infinite matter or the zero range approximations, or it may be that multiple collisions are important.

I. INTRODUCTION

Photon production rates provide a clean probe of nuclear reaction dynamics because of the weakness of the electromagnetic coupling. Of course, cross sections are small for high energy photons, but experimental techniques allow measurements for photons much higher in energy than the giant dipole resonance.[1–5] These ultradipole photons hold promise to tell us about the early stages of the nuclear reaction, when the energy is not yet disbursed over many degrees of freedom. Our goal here is to clarify some mechanisms of ultradipole photon production, to facilitate the interpretation of measurements in terms of fundamental quantities of nuclear dynamics. Theories of photon production can be divided into two main approaches, either based on an assumed statistical equilibrium or based on detailed models of the nuclear currents. If the statistical limit occurs, measurements convey information about the time duration of the collision and the density of states at high excitation. If the coherent currents in the early stages of the collision are most important, the measurement tells us about the charge deceleration process, at least for photon energies below 100 MeV. In this work we will examine the coherent dynamics of the early stages of the collision, and obtain some numerical estimates of the predicted photon production.

The most well-founded theory of nuclear dynamics is based on separating the Hamiltonian into a part describing single-particle motion in a mean field and the remainder treated as a two-body residual interaction. These two kinds of interaction provide two bremsstrahlung mechanisms that we will analyze in this paper. The potential field mechanism is well known in low energy nuclear physics as the direct capture mechanism in radiative nucleon capture. For heavy ion reactions, potential field effects are most reliably calculated using the time-dependent Hartree-Fock (TDHF) theory. Bauer *et al.*[6] studied photon production by this mechanism for ^{12}C induced reactions at 84 MeV/N bombarding energy, and found yields to be an order of magnitude smaller than the data.[3] The collisional bremmstrahlung mechanism has been considered for heavy ion reactions by Nifenecker and Bondorf[7] and by Ko *et al.*[8] Nifenecker and Bondorf made analytic estimates of the rates, separating the bremsstrahlung into coherent and incoherent parts, and also separating the entrance channel contribution from the rest. They find that the incoherent bremsstrahlung from pn collisions dominates for the conditions they studied. They were also able to explain the magnitude of the cross section in Ref. 3 estimating the nucleons to make 20—30 collisions apiece. Ko *et al.* applied a nuclear cascade model to intermediate energy heavy ion collisions, and found that the incoherent pn collisions were most important except for high-Z projectiles and targets. In these systems the coherent bremsstrahlung from the collective deceleration of the target, with its characteristic quadrupolar radiation pattern, becomes significant. Collective deceleration as a source of bremsstrahlung was the mechanism first considered in phenomenological models.[9–11]

To disentangle the basic questions about the important mechanisms from the geometric complications of finite nuclei, we will here calculate the processes in infinite nuclear matter. As will be seen, this makes the calculations quite straightforward and transparent, but the cost is that shell effects will be beyond the scope of the theory. Shell effects are crucial for the giant dipole resonance, but we believe that they are unnecessary to describe smooth or averaged cross sections. This has been the experience in applying semi-infinite nuclear matter results to the response of finite nuclei.[12]

In the next two sections we derive estimates for the photon production rates in infinite nuclear matter by the two mechanisms. We then show how to apply these results to finite nuclear geometry. Finally, we discuss some of the available experimental data.

II. BREMSSTRAHLUNG FROM THE POTENTIAL FIELD

The photon production rate is derived conveniently from Fermi's golden rule for the transition rate. The probability of emitting a photon of momentum k is expressed in terms of the transition rate and the matrix element of the electromagnetic interaction as

$$dP=\frac{dW}{\phi}=\frac{2\pi}{\phi}\,|\langle\psi_i,0\,|\,\mathbf{j}\cdot\mathbf{A}\,|\,\psi_f,k\rangle|^2\frac{dn_f dn_k}{dE}\ . \tag{2.1}$$

Here, ψ_i and ψ_f are the incident and final wave functions, ϕ is the flux of the incident beam, and dn_f and dn_k are the densities of nuclear final states and photon final states. With this formula there always seems to be the possibility of confusion by a factor of 4π due to the choice of electromagnetic units. We will specify units by setting $\hbar=c=1$, and defining the charge e so that the current is related to velocity by $\mathbf{j}=e\mathbf{v}$ and the fine structure constant is $e^2=\alpha=\frac{1}{137}$. We normalize the photon states so that the matrix element to create a photon is

$$\langle 0\,|\,\mathbf{A}\,|\,k\rangle=\sqrt{2\pi/\omega}\,\hat{\boldsymbol{\epsilon}}_k e^{i\mathbf{k}\cdot\mathbf{r}}\ , \tag{2.2}$$

where ω is the energy of the photon and $\hat{\boldsymbol{\epsilon}}_k$ is a unit polarization vector. The density of photon states in this normalization is

$$dn_k=\frac{\omega^2 d\omega\, d\Omega}{(2\pi)^3}\ . \tag{2.3}$$

The potential field acceleration mechanism will be calculated by taking the proton wave function to be an eigenstate of the one-dimensional potential well

$$V(z)=\frac{V_0}{1+\exp(z/a)},\quad V_0=-50\text{ MeV},\quad a=0.65\text{ fm}\ . \tag{2.4}$$

We choose to normalize ψ_i to one particle per unit volume incident on the potential well. The initial wave function then has the asymptotic behavior

$$\psi_i=\begin{cases}e^{ip_i z}+r_i e^{-ip_i z}, & z\ll 0\\ t_i e^{ip_i' z}, & z\gg 0\ .\end{cases} \tag{2.5}$$

Here, p_i and p_i' are the momenta of the proton before and after crossing the potential. The relation to the incident energy is

$$E_i=\frac{p_i^2}{2m}=\frac{(p_i')^2}{2m}+V_0\ . \tag{2.6}$$

Also, in Eq. (2.5), r and t are reflection and transmission amplitudes which satisfy

$$r^2+\frac{p_i'}{p_i}t^2=1\ .$$

The transverse dimensions of the system will be taken to make a unit cross sectional area, so the flux factor in Eq. (2.1) is

$$\phi=p_i/m\ . \tag{2.7}$$

The final state will be normalized to one particle per unit volume on the left-hand side of the potential,

$$\psi_f^{\pm}=\begin{cases}e^{\pm ip_f' z}, & z\gg 0\\ \frac{1}{t_f}e^{ip_f z}+\frac{r_f}{t_f}e^{-ip_f z}, & z\ll 0\end{cases} \tag{2.8a}$$

where

$$\frac{(p_f')^2}{2m}=\frac{(p_i')^2}{2m}-\omega,\quad \frac{p_f^2}{2m}=\frac{p_i^2}{2m}-\omega\ .$$

A sum over final states including both $(+)$ and $(-)$ asymptotic states is required to calculate the total bremsstrahlung rate. When the final state is bound by the potential, the asymptotic form changes to

$$\psi_f^b=e^{+ip_f' z}-e^{i\eta}e^{-ip_f' z},\quad z\gg 0,\quad \frac{(p_f')^2}{2m}<V_0\ . \tag{2.8b}$$

With these normalizations, the density of final nucleon states for both bound and unbound states is given by

$$dn_f=\frac{dp_f'}{2\pi}=\frac{m}{2\pi p_f'}dE_f\ . \tag{2.9}$$

Combining these relations, we arrive at the formula for the probability of photon emission per unit solid angle and unit photon energy,

$$\frac{d^2P}{d\omega\, d\Omega}=\frac{\alpha\omega}{(2\pi)^2}\frac{m^2}{p_i p_f'}\sum_{\epsilon}^{2}\left|\int dz\,\psi_i^*(z)e^{ik_z z}\frac{\mathbf{p}}{m}\hat{\boldsymbol{\epsilon}}_k\psi_f(z)\right|^2\ . \tag{2.10}$$

Before applying this formula to the Woods-Saxon eigenfunctions, it is useful to evaluate it in the semiclassical limit. To obtain this limit we approximate ψ_i and ψ_f by WKB wave functions. We also assume that the photon energy is very small, in which case the asymptotic regions dominate in the integration. It is a simple exercise left to the reader to show that Eq. (2.10) then reduces to

$$\frac{d^2P}{d\omega\, d\Omega}=\alpha\frac{1}{(2\pi)^2\omega}\sum_{\epsilon}\left|\frac{\mathbf{v}_i\cdot\hat{\boldsymbol{\epsilon}}_k}{1-\mathbf{v}_i\cdot\hat{\mathbf{k}}}-\frac{\mathbf{v}_f\cdot\hat{\boldsymbol{\epsilon}}_k}{1-\mathbf{v}_f\cdot\hat{\mathbf{k}}}\right|^2\ . \tag{2.11}$$

Here, $v_{i,f}=p_{i,f}/m$ are the velocities of the particle before and after crossing the potential step. Equation (2.11) is just the classical bremsstrahlung equation. Equation (2.11) does not apply to photon energies large enough for capture. A better analytic formula can be obtained by using the eigenfunctions of the step potential. Then the wave function is given exactly by Eqs. (2.5) and (2.8a) with the following transmission and reflection coefficients,

$$t_i=\frac{2}{1+p_i'/p_i},\quad r_i=\frac{1-p_i'/p_i}{1+p_i'/p_i}\ . \tag{2.12}$$

The matrix element can then be evaluated exactly to give

$$\frac{d^2P}{d\omega\, d\Omega}=\frac{\alpha\omega}{(2\pi)^2 p_i p_f'}\sum_{\epsilon,\pm p_f'}(\hat{\epsilon}_k\cdot\hat{z})^2\left[\frac{p_i+p_f}{2t_f(p_f-p_i+k_z)}+\frac{r_f}{2t_f}\frac{p_i-p_f}{-p_f-p_i+k_z}\right.$$

$$\left.+\frac{r_i r_f}{2t_f}\frac{-p_i-p_f}{-p_f+p_i+k_z}+\frac{r_i}{2t_f}\frac{-p_i+p_f}{p_f+p_i+k_z}-\frac{t_i(p_i'+p_f')}{2(p_f'-p_i'+k_z)}\right]^2 . \tag{2.13}$$

The corresponding formula for transitions to bound final states is

$$\frac{d^2P}{d\omega\, d\Omega}=\frac{\alpha\omega}{(2\pi)^2 p_i p_f'(p_f'^2+p_f^2)}\sum_{\epsilon}(\hat{\epsilon}_k\cdot\hat{z})^2\left|\frac{p_f' p_f}{p_f-ip_i+ik_z}+\frac{r_i p_f' p_f}{p_f+ip_i+ik_z}-\frac{t_i p_f'(p_f'-ip_f)}{2(p_f'-p_i'+k_z)}+\frac{t_i p_f'(p_f'+ip_f)}{2(-p_f'-p_i'+k_z)}\right|^2 , \tag{2.14}$$

where p_f in this case satisfies

$$\frac{p_f^2}{2m}=\omega-\frac{p_i^2}{2m} .$$

Unfortunately, the sharp-edged potential does not give accurate estimates for the Woods-Saxon wave functions, so it is necessary to evaluate the integral numerically. This is not quite a trivial task because of the lack of uniform convergence of the integral. A practical way to handle this problem is to choose finite limits for the integral, placed in the asymptotic regions of the wave functions. The contributions between the limits is calculated numerically and the contribution from outside is added analytically.[13] Our method of treating the limits allows a simple check on the computer program. The result will be independent of the integration limits only if the analytic contributions are included correctly and the numerical integration is sufficiently accurate.

The numerically calculated bremsstrahlung rate for 40 MeV protons is shown in Fig. 1, compared with the rate for the corresponding sharp-edged potential, Eqs. (2.13) and (2.14). There is a large discontinuity in the sharp-edged result when the final state becomes bound, but this is reduced much more in the realistic case. Overall, the rate is lower in the realistic case. The spectrum approaches $1/\omega$ for transitions between unbound states, but falls off more rapidly in the bound state region. It is useful to display the rate as a function of beam energy, holding the photon energy fixed, for our later application to finite nuclear geometry. This is shown in Fig. 2, for a range of photon energies between 30 and 60 MeV. We see that the rate is nearly flat in the vicinity of the capture threshold. For a rough estimate of the rate, we can ignore the dependence on beam energy and parametrize the photon energy dependence as

$$\frac{d^2P}{d\omega\, d\Omega}\approx 1.6\times10^{-7}\ (\mathrm{MeV\,sr})^{-1}\left[\frac{30\ \mathrm{MeV}}{\omega}\right]^{2.5} ,$$

$$30\le\omega\le 60\ \mathrm{MeV} . \tag{2.15}$$

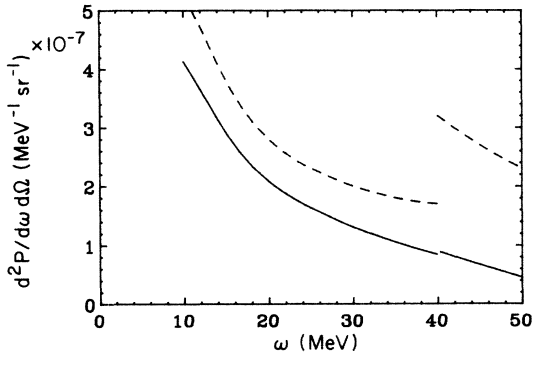

FIG. 1. Bremsstrahlung probability from a 40 MeV proton crossing a Woods-Saxon potential of 50 MeV depth, with the photon emitted perpendicular to the incident proton direction. The dashed line shows the result for a sharp-edged well, which is given analytically by Eqs. (13) and (14). Note the discontinuous jump for captured protons. The solid line shows the result for a realistic diffusivity of the potential, $a=0.65$ fm.

III. COLLISIONAL BREMSSTRAHLUNG IN PROTON-INDUCED REACTIONS

We consider only collisions between neutrons and protons. Proton-proton bremsstrahlung is smaller by an or-

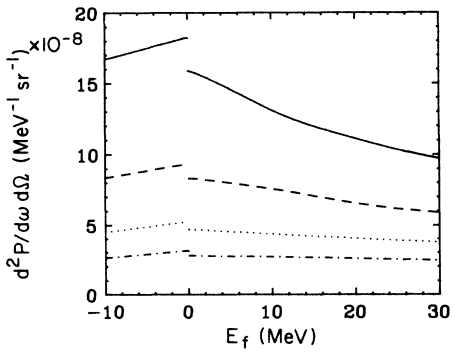

FIG. 2. Potential well bremsstrahlung rate from Eq. (2.10) shown as a function of final proton energy. The solid, dashed, dotted, and dashed-dotted curves correspond to the photon energies of 30, 40, 50, and 60 MeV, respectively.

der of magnitude because the radiation is quadrupolar rather than dipolar. We first consider a single proton moving through infinite nuclear matter. It will eventually scatter from one of the nucleons in the Fermi sea, and it may or may not emit a photon in the process. For the creation of energetic photons, we need only consider this first-chance bremsstrahlung rate. After the first collision, the energy of the proton is degraded, reducing the probability of making energetic photons in subsequent collisions. In perturbation theory the bremsstrahlung rate may be calculated from the second order formula

$$dW_{\mathrm{pn}\gamma}=2\pi\left|\langle\psi_{ij}0\,|\,\mathbf{j}\cdot\mathbf{A}\frac{1}{E_i-H_o}V+V\frac{1}{E_i-H_0}\mathbf{j}\cdot\mathbf{A}\,|\,\psi_{fj}q\rangle\right|^2\frac{dn_f dn_q}{dE}\,. \tag{3.1}$$

Here, ψ_i and ψ_f are many-particle states composed of plane wave single-particle wave functions. The residual interaction between two particles is V. The sum over intermediate states reduces to a single term in the plane wave representation because of momentum conservation. The graphical representation of the second order amplitude is shown in Fig. 3, defining the momentum labels we use below. One technical point that should be mentioned is that gauge invariance requires an additional amplitude to be added when the interaction is nonlocal, due to the currents contained in the interaction. The correction is small for n-p bremsstrahlung and we neglect it.

The collisional rate of the incident proton irrespective of the bremsstrahlung is given by

$$W_{\mathrm{pn}}=2\pi\,|\,\langle\psi_i\,|\,V\,|\,\psi_f\rangle\,|^2\frac{dn_f}{dE}\,. \tag{3.2}$$

The bremmstrahlung probability is just the ratio of (3.1) to (3.2). While the individual rates are sensitive to the absolute strength of the residual interaction, the ratio is independent. Thus the bremsstrahlung probability can be calculated without very precise knowledge of the interaction. We shall make the simple assumption that the interaction is independent of energy and momentum transfer, i.e., it can be replaced by a delta function,

$$V=v_0\delta^3(r_{\mathrm{p}}-r_{\mathrm{n}})\,. \tag{3.3}$$

In free np scattering, the probability would be evaluated using the free t matrix. This has a strong energy dependence (in fact, a pole at the deuteron energy), but in nuclear matter the Pauli exclusion will reduce the variation of a G-matrix interaction.

To exhibit the formula for the bremsstrahlung rate, we define momentum variables p_1, p_2, p_3, and p_4 of the initial proton, initial neutron, final proton, and final neutron. Using relativistically correct energies and matrix elements of the current operator, the formula is

$$\frac{d^2W_{\mathrm{pn}\gamma}}{d\omega\,d\Omega}=\frac{\alpha v_0^2}{2\pi\omega}g\int_{<k_F}\frac{d^3p_2}{(2\pi)^3}\int\frac{d^3p_3}{(2\pi)^3}Q\,\delta(\epsilon_1+\epsilon_2-\epsilon_3-\epsilon_4-\omega)\left|\frac{\hat{\boldsymbol{\epsilon}}\cdot\mathbf{v}_3}{1-\hat{\mathbf{k}}\cdot\mathbf{v}_3}-\frac{\hat{\boldsymbol{\epsilon}}\cdot\mathbf{v}_1}{1-\hat{\mathbf{k}}\cdot\mathbf{v}_1}\right|^2, \tag{3.4}$$

where $g=2$ is the spin degeneracy of the Fermi sea. The variables are defined analogously to Eq. (2.11). The sum over final states is restricted by the Pauli blocking operator Q. For a single nucleon in nuclear matter, Q simply excludes the target Fermi sphere,

$$Q=\Theta(p_3-p_F)\Theta(p_4-p_F),\quad \mathbf{p}_4=\mathbf{p}_1+\mathbf{p}_2-\mathbf{p}_3\,. \tag{3.5}$$

The phase space occupancy is different for heavy ion collisions, and the Pauli operator will have to be modified to describe that situation. We will return to that later. The energy conserving delta function reduces the integration over the final proton momentum $\mathbf{p}_3$ to an angular integration.

In order to obtain the differential probability $d^2P/d\omega\,d\Omega$, we divide Eq. (3.4) by the total collision rate. The pn collision probability is given by

$$W_{\mathrm{pn}}=2\pi v_0^2 g\int_{<k_F}\frac{d^3p_2}{(2\pi)^3}\int\frac{d^3p_3}{(2\pi)^3}Q\,\delta(\epsilon_1+\epsilon_2-\epsilon_3-\epsilon_4)\,. \tag{3.6}$$

We assume that pp collisions are as likely as pn collisions, and divide Eq. (3.4) by twice (3.6) to obtain the probability distribution

$$\frac{d^2P}{d\omega\,d\Omega}=\frac{1}{2W_{\mathrm{pn}}}\frac{d^2W_{\mathrm{pn}\gamma}}{d\omega\,d\Omega}=\frac{\alpha}{(2\pi)^2\omega}\frac{\int_{<k_F}d^3p_2\int d^3p_3 Q\,\delta(\epsilon_1+\epsilon_2-\epsilon_3-\epsilon_4-\omega)\left|\frac{\hat{\boldsymbol{\epsilon}}\cdot\mathbf{v}_3}{1-\hat{\mathbf{k}}\cdot\mathbf{v}_3}-\frac{\hat{\boldsymbol{\epsilon}}\cdot\mathbf{v}_1}{1-\hat{\mathbf{k}}\cdot\mathbf{v}_1}\right|^2}{2\int_{<k_F}d^3p_2\int d^3p_3 Q\,\delta(\epsilon_1+\epsilon_2-\epsilon_3-\epsilon_4)}\,. \tag{3.7}$$

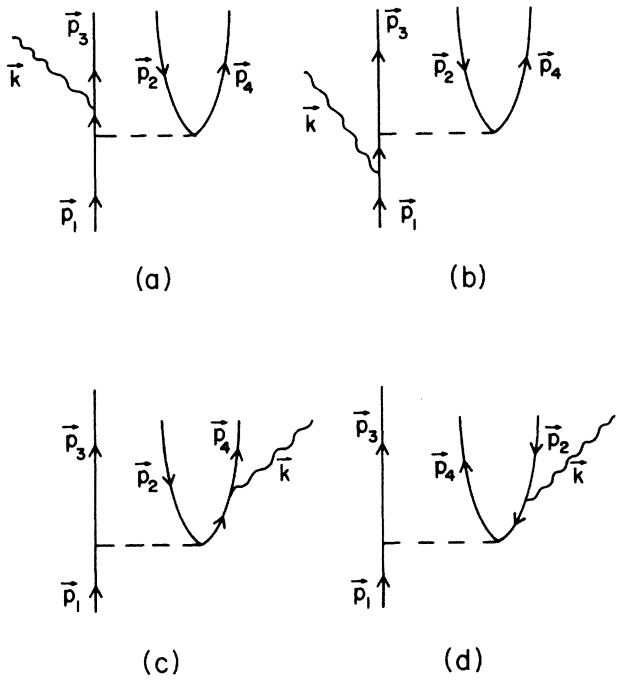

FIG. 3. Perturbation diagrams for the bremsstrahlung in collisions of nucleons in nuclear matter.

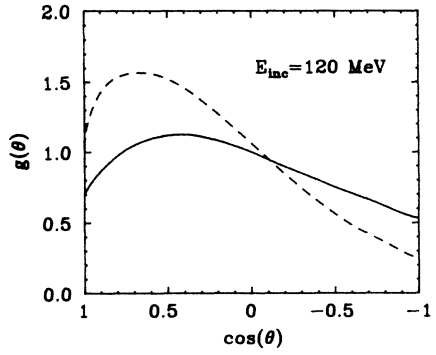

FIG. 4. Angular distribution of photons from proton-neutron bremsstrahlung in nuclear matter, normalized at 90°. The proton has a kinetic energy of 120 MeV in the medium, and the Fermi energy is 38 MeV. The distribution in the mid-velocity frame and the lab frame are shown by the solid and dashed lines, respectively.

This is the basic formula we evaluate in this section. The numerator requires a fivefold integration, which we performed numerically. Before discussing the results of the numerical evaluation of (3.7), we remark on the connection to classical treatments of collisional bremsstrahlung. Classical theory results if we assume that the integrations in the numerator and denominator of (3.7) cancel out, leaving an average over the squared term. That approximation does not treat the final state phase space well, because the density of final states is a rapid function of the photon energy. Even in the simplest case, without any Pauli blocking, the final state phase space introduces an additional factor k'/k, where k and k' are the initial and final momentum in the nucleon-nucleon c.m. frame.[8]

We now examine the angular distribution predicted by Eq. (3.7). The result for an incident energy of 120 MeV is shown in Fig. 4. To interpret it, we note that the angular distribution for nonrelativistic neutron-proton collisions has a dipolar character. The incoming current along the z axis produces a $\sin^2\theta$ angular distribution, while the outgoing current permits a $\cos^2\theta$ contribution as well. The specific shape of the angular distribution in proton-neutron scattering is easily evaluated assuming an isotropic cross section and low energy photons. We define an angular distribution function $g(\theta)$ normalized to 1 at a 90° scattering angle. The free scattering result in the c.m. frame is

$$g(\theta)=0.6\sin^2\theta+0.4\ . \tag{3.8}$$

To compare with the nucleon-nuclear matter bremsstrahlung, we evaluate its angular distribution in a frame having a velocity midway between the proton and the nuclear matter target. This is shown as the solid line in Fig. 4. The anisotropy is weaker than obtained in free np collisions, Eq. (3.8). There are two effects operating that reduce the anisotropy. One is the Pauli principle, which favors collisions having a large transverse momentum transfer. The anisotropy is also reduced by the averaging over incident momentum directions due to the Fermi motion of the target neutron. There is also an asymmetry about 90° due to the near-relativistic velocity of the proton, which invalidates the dipole approximation. The angular distribution may be transformed to another frame using the formula

$$\frac{d^2P}{d\omega\, d\Omega}=\frac{\omega}{\omega'}\frac{d^2P}{d\omega' d\Omega'}\ .$$

Here, ω,ω' are the proton energies and Ω,Ω' are the angles in the two frames. In the lab frame the transformation results in a considerable forward peaking of $g(\theta)$. The distribution is shown as the dashed line in Fig. 4. The forward peaking is to be expected when the projectile velocity becomes of the order of $c/2$, as is the case here.

Some qualitative features of the ω dependence of Eq. (3.5) may be extracted from the behavior near extremes. For low photon energies, the dependence is the usual bremsstrahlung $1/\omega$. Near the maximum photon energy, the rate is proportional to the final state phase space. In the Fermi gas model the density of states of a given particle-hole character varies as a power of the excitation energy. In the case of Fig. 3 the final state has a two-particle one-hole character, which has a quadratically varying density of states near the Fermi level.[14] Thus close to the endpoint the bremsstrahlung rate will depend on ω as $dP/d\omega\propto(\omega_{\max}-\omega)^2$. We can combine the extremal behavior into a single function, given by Eq. (3.9) below. This reproduces very well the numerical evaluation of Eq. (3.6) for proton energies in the range 40—150 MeV:

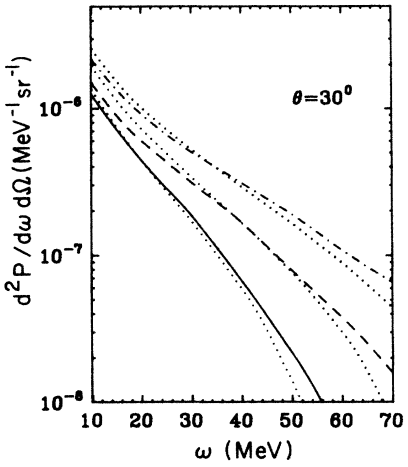

FIG. 5. Energy distribution of bremsstrahlung photons from the proton collisions in nuclear matter. Incident proton energies of 100, 120, and 140 MeV are shown by the solid, dashed, and dotted-dashed curves, respectively. The dotted curves show the analytic fit from Eq. (3.9).

$$\frac{d^2P}{d\omega\, d\Omega}=2.5\times10^{-7}g(\theta)\frac{(\omega_{\max}-\omega)^2}{\omega_{\max}\omega}\ \mathrm{MeV}^{-1}\ . \quad (3.9)$$

This is illustrated in Fig. 5, showing the numerical evaluation of Eq. (3.6) for a variety of energies.

IV. APPLICATION TO FINITE NUCLEAR GEOMETRIES

The results found above are applied to finite nuclei by assuming that the nucleus can be divided into small noninterfering regions, each of which approximates nuclear matter. The neglected interferences give rise to shell effects which are ignored, as was mentioned before.

For the potential well bremsstrahlung, we need to average over the spherical geometry of the potential edge. The acceleration of the proton is in the direction normal to the target surface, so we may apply the formula given by Eq. (2.10) to the normal component p_n of the incident momentum p_i and average over impact parameter b. This yields the following integral,

$$\frac{d^2\sigma}{d\omega\, d\Omega}=\int_0^R d^2b\frac{d^2P}{d\omega\, d\Omega}\left[E=\frac{p_n^2}{2m}\right]|\hat{\epsilon}\cdot\hat{\mathbf{p}}_n|^2\ , \quad (4.1)$$

where

$$p_n=p_i\cos\theta'=p_i[1-(b/R)^2]^{1/2}$$

and θ' is the polar angle on the nuclear surface where the proton crosses into the nucleus. R is the radius of the nucleus. As discussed in Sec. II, we will estimate the rate taking $d^2P/d\omega\, d\Omega$ to be independent of proton energy for fixed ω. The Pauli principle prevents capture to states more bound than the separation energy, which enforces a limit on the maximum photon energy. The only dependence on the geometry left is in the polarization factor. The integration over azimuthal angle yields

$$\sum_\epsilon\int d\phi\,|\hat{\epsilon}_k\cdot\hat{\mathbf{p}}_n|^2 \cdot=2\pi\left\{\left[1-\left[\frac{b}{R}\right]^2\right]\sin^2\theta+\frac{1}{2}\left[\frac{b}{R}\right]^2(1+\cos^2\theta)\right\}, \quad (4.2)$$

where θ is the angle of the gamma ray with respect to the beam axis. We now perform the integration over impact parameter, obtaining

$$\int b\,db\sum_\epsilon\int d\phi\,|\hat{\epsilon}_k\cdot\hat{\mathbf{p}}_n|^2=\pi R^2(\tfrac{1}{2}+\tfrac{1}{4}\sin^2\theta)\ , \quad (4.3)$$

where R is the target radius. The formula shows a somewhat more isotropic angular distribution than the collisional bremsstrahlung. The transverse acceleration from the potential field in near-grazing trajectories provides an important source for the photons.

There is one correction we have to make to the current operator before it can be applied to finite nuclei. There is a contribution to the current due to the velocity of the target. Momentum conservation fixes the magnitude of the velocity (in the c.m. frame) at $-1/A$ times the proton velocity. The total current is then given by

$$\langle j\rangle_T=\left[1-\frac{Z}{A}F(q)\right]\langle j\rangle_p\ , \quad (4.4)$$

where $F(q)$ is the form factor of the target for photons of momentum q, normalized to $F(0)=1$. The final formula for the potential-well induced bremsstrahlung is then

$$\left.\frac{d^2\sigma}{d\omega\, d\Omega}\right|_{\mathrm{pot}}\approx1.2\times10^{-7}\left[\frac{30\ \mathrm{MeV}}{\omega}\right]^{2.5}\pi R^2(\tfrac{2}{3}+\tfrac{1}{3}\sin^2\theta)\left[1-\frac{Z}{A}F(q)\right]^2,\quad 30\le\omega\le60\ \mathrm{MeV}\ . \quad (4.5)$$

We next apply the nuclear matter model of the collisional bremsstrahlung to finite nuclei. This is quite simple if we assume that the target is thick enough so that nucleon-nucleon collisions will occur with a high probability. Then the bremsstrahlung probability from Eq. (3.9) is multiplied by the geometric cross section to obtain

$$\left.\frac{d^2\sigma}{d\omega\, d\Omega}\right|_{\mathrm{col}}\approx2.5\times10^{-7}g(\theta)\pi R^2\frac{(\omega_{\max}-\omega)^2}{\omega_{\max}\omega}\ \mathrm{MeV}^{-1}\ , \quad (4.6)$$

where R is the radius of the target and $g(\theta)\approx1$. Compar-

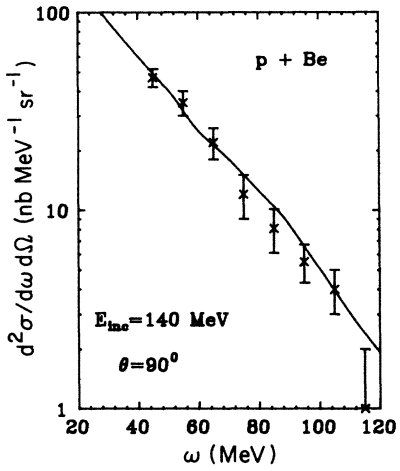

FIG. 6. Bremsstrahlung cross section in the p + Be reaction at 140 MeV incident energy, for photon emission angle of 90°. The solid line is our prediction. The data are from Ref. 1.

ing Eqs. (4.5) and (4.6), we see that the collisional bremsstrahlung is the more likely process, for the ω range 30—60 MeV, and proton bombarding energies in the range 80—150 MeV.

Measurements of high energy photons produced in 140 MeV proton reactions have been reported in Ref. 1. A broad range of targets was studied, and cross sections were measured for photon energies in the range of 40 MeV to over 100 MeV. In the range of 40—60 MeV the collisional bremsstrahlung should dominate the cross section. Figure 6 shows the comparison of the observed energy spectrum with the prediction for a Be target at $\theta=90°$. We have assumed a potential well depth of 50 MeV and a Fermi energy of 38 MeV in the theoretical cross section. The agreement is excellent, showing that the first collision accounts for most of the cross section. Reference 1 also quotes total cross sections which can be easily obtained by integrating Eq. (4.6) over the momentum of the photon. For Pb targets and photon energies over 30 MeV, this yields $\sigma=250$ μb, which is again in good agreement with the observed yield of 225 ± 25 μb. Finally, the observed cross section scales with target mass as $A^{2/3}$, as expected from any direct production mechanism.

V. NUCLEUS-NUCLEUS BREMSSTRAHLUNG

The phase space distribution of nucleons in a collision between nuclei is much more complicated than for the proton reactions. However, on a qualitative level, the momentum space distribution obtained with mean field theory is fairly simple to describe. The nuclear potential is relatively insensitive to the density near the saturation value, so the nucleons of the projectile are not appreciably accelerated upon going into the target.[15,16] The projectile momentum space distribution is then close to the original sphere, displaced from the Fermi sphere of the target by the momentum per particle of the incident beam. Of course, the nucleon occupation factor remains unity in the intersection region of the two spheres. We shall assume this double sphere geometry for our estimates of the bremsstrahlung. Due to the Fermi motion, the effective energy of the nucleons at the tips of the Fermi spheres is much higher than the beam energy. The effective maximum energies (with respect to the target Fermi sphere) for heavy ion beam energies of 25—50 MeV/N range from 75 to 125 MeV, neglecting Coulomb effects. Thus the proton-nucleus bremsstrahlung considered in the preceding section is in a good kinematic range to compare with photon production in heavy ion collisions.

Since the particles are not accelerated by the potential field in the initial stages of the collision, the potential well bremsstrahlung will be even weaker than in the proton reactions. The deceleration really only begins when the nucleons from the projectile arrive at the far surface of the target. A single nucleon may jump over the potential well on the far side, keeping most of the kinetic energy it had originally. Because of the Fermi momentum, the final energy could be much higher than the beam energy per particle. However, there would not be much bremsstrahlung produced, because only a small fraction of the projectile nucleons can be emitted this way. After the first nucleons reach the farther potential barrier, the potential field responds to the additional nucleons and moves with them. So we feel confident in ignoring the potential field bremsstrahlung entirely.

To estimate the collisional bremsstrahlung, we first consider the bremsstrahlung transition rate $d^2W/d\omega\, d\Omega$ for an individual proton in the projectile nucleus. The formula to be evaluated is the same as Eq. (3.4), except that here the Pauli blocking operator Q is modified to properly account for the double sphere geometry,

$$Q=\Theta(p_3-p_F)\Theta(p_4-p_F)\Theta(|\mathbf{p}_3-m\mathbf{v}|-p_F) \times\Theta(|\mathbf{p}_4+m\mathbf{v}|-p_F)\,, \tag{5.1}$$

where $\mathbf{v}$ is the beam velocity. Because the Pauli blocking is much more effective in the double sphere geometry, we cannot assume that every proton will make a collision. Instead, we define a decay time τ for the initial momentum distribution and obtain the differential probability by integrating the rate over time,

$$\frac{d^2P}{d\omega\, d\Omega}=\int_0^{\tau_{\rm trans}} dt\, \frac{d^2W}{d\omega\, d\Omega}e^{-t/\tau}\,. \tag{5.2}$$

If the collision rate is low, the time duration is determined by $\tau_{\rm trans}$, the transit time of a nucleon across the target nucleus. We shall estimate this as $\tau_{\rm trans}=2R/v$, where R is the radius of the target and v is the nucleon velocity. If the collision rate is high, the double sphere geometry will degrade into a thermal distribution before the compressed phase of the collision is over. The time available for first-collision bremsstrahlung will then be determined by the thermalization rate.

We shall apply Eq. (5.2) taking the thermalization time τ to be the inverse rate for the particle to collide with others. We then sum over particles in the projectile, and average over their momentum distribution. We include both neutrons and protons in the sum: pn bremsstrahlung

TABLE I. Each ingredient in Eq. (5.4) as a function of the z component (direction of the incident beam moment) p_z of the momentum of the projectile particle in the Fermi distribution. The first column is p_z in units of fm^{-1}. The second column is the phase space available for a given p_z [ratio between the volume $\Delta V(p_z)$ for a given p_z and the total volume $V=4\pi k_F^3/3$]. The third column is the transition probability of making a photon in units of $(\mathrm{fm\,MeV\,sr})^{-1}$. The fourth column is the total nucleon-nucleon collision rate in units of fm^{-1}, whose inverse is the mean lifetime $\tau(p_z)$. The fifth column gives the probability of a projectile nucleon with momentum p_z to suffer a collision. Finally, the last column is the integrand in Eq. (5.4) multiplied by the phase space factor. All the ingredients are calculated for incident energy of 40 MeV/N and photon energy of 30 MeV. The photon emission angle is $\theta=0°$.

p_z	$\frac{\Delta V(p_z)}{V}$	$\frac{d^2W}{d\omega\,d\Omega}(p_z)$	$W(p_z)$	$(1-e^{-\tau_{\mathrm{trans}}/\tau(p_z)})$	$\frac{\Delta V(p_z)}{V}\left[\frac{\frac{d^2W}{d\omega\,d\Omega}(p_z)}{W(p_z)}\right](1-e^{-\tau_{\mathrm{trans}}/\tau(p_z)})$
1.26	1.71×10^{-2}	4.72×10^{-8}	1.25×10^{-1}	1	6.41×10^{-9}
1.05	4.71×10^{-2}	3.69×10^{-8}	1.08×10^{-1}	0.99	1.60×10^{-8}
0.84	7.17×10^{-2}	1.96×10^{-8}	8.49×10^{-2}	0.98	1.63×10^{-8}
0.63	9.08×10^{-2}	1.10×10^{-8}	5.38×10^{-2}	0.92	1.72×10^{-8}
0.42	1.04×10^{-1}	5.07×10^{-9}	3.22×10^{-2}	0.79	1.29×10^{-8}
0.21	1.13×10^{-1}	6.39×10^{-10}	2.12×10^{-2}	0.64	2.17×10^{-9}
0	1.15×10^{-1}	0	1.24×10^{-2}	0.45	0

can arise from either species in the projectile. We also integrate over time to obtain the formula we use in the calculations,

$$\frac{d^2P}{d\omega\,d\Omega}=A\int_{<k_F}\frac{d^3p_1}{\frac{4\pi}{3}k_F^3}\frac{\frac{d^2W}{d\omega\,d\Omega}(p_1)}{W(p_1)}(1-e^{-\tau_{\mathrm{trans}}/\tau})\,. \tag{5.3}$$

Here, A is the number of nucleons in the projectile. In deriving this formula, we have ignored the decay of the target sphere momentum distribution. Thus Eq. (5.3) will include some contributions from collisions in which the target particle has already undergone a collision. Our results will therefore overestimate the first-chance collision rate. A more refined estimate, treating the target and projectile nucleons on an equal footing, may be obtained using the method of Ref. 17. However, this requires an explicit integration of the transition rate per unit volume over the volume of the interpenetrating nuclei. For our purposes here, a simpler estimate is more desirable.

With the compact geometry of the double Fermi sphere, the NN collision rate may not be high enough to assure that all particles capable of producing bremsstrahlung will make a collision. We have therefore explicitly included the dependence on the transit time of the projectile nucleons in Eq. (5.3). To study this point more closely, we examine the contributions to Eq. (5.3) as a function of the longitudinal momentum of the projectile particle. We assume a residual interaction strength of 300 $\mathrm{MeV\,fm}^3$, which is equivalent to a NN cross section of 40 mb. The actual free NN cross section is larger, but the medium corrections of Brueckner theory reduce the effective interaction strength. We have taken as a typical case interactions with a ^{208}Pb target, at a projectile energy of 40 MeV/N. We estimate the transit time as

$$\tau_{\mathrm{trans}}=2(R=7\ \mathrm{fm})/(v=0.3c)=50\ \mathrm{fm}/c\ .$$

The nucleon-nucleon collision rates and the bremsstrahlung rates for 30 MeV photons at the emission angle of $\theta=30°$ are displayed in Table I. The various rates are also shown. The decay times range from 8 fm/c for a particle near the tip of the momentum distribution to 47 fm/c for particles near the bottom of the momentum range contributing to the bremsstrahlung. The thermalization time computed in Ref. 18, given as a function of bombarding energy as $\tau=1000/E_{\mathrm{lab}}$, yields 25 fm/$c$. The thermalization estimate of Ref. 19, which is much smaller, agrees with the time for the tips of the Fermi distribution to decay. In any case, the decay rate is fast enough that the last exponential term in Eq. (5.3) may be neglected for all but the smallest radius targets.

The predicted angular distribution from Eq. (5.3), normalized to 1 at 90°, is shown in Fig. 7 for an incident energy of 40 MeV/N and a photon energy of 30 MeV. The solid curve displays the result in the mid-velocity frame, which is necessarily symmetric about 90°. The angular

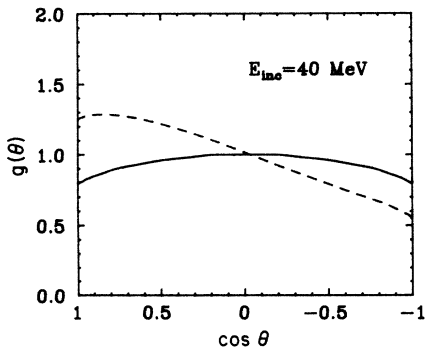

FIG. 7. Angular distribution of collisional bremsstrahlung photons for a heavy ion reaction at an incident energy of 40 MeV/N. The photon energy is 30 MeV. The distribution in the mid-velocity frame and the lab frame are shown by solid and dashed lines, respectively.

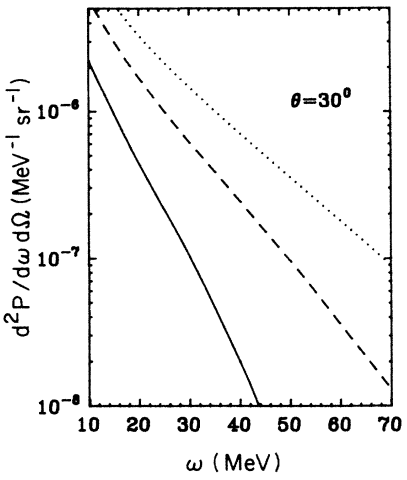

FIG. 8. Energy distribution of collisional bremsstrahlung photons for heavy ion reactions with heavy targets, calculated with Eq. (5.3). The incident energies are 20, 40, and 60 MeV/N for the solid, dashed, and dotted curves, respectively, and the cross section is shown for the mid-velocity frame.

distribution in the lab frame is given by the dashed curve. There is a considerable forward peaking as in the case of the proton induced bremsstrahlung.

The ω dependence of Eq. (5.3) is shown in Fig. 8 for several incident energies. The dependence on incident energy is stronger than in the proton-nucleus case because Pauli blocking of phase space is more severe at low energies for heavy ion collisions. The dependence on photon energy near the maximum is also more rapid than in the previous case. According to the argument given in Sec. III, we might expect a threshold dependence of the form $(\omega_{\max}-\omega)^3$ since the final state has two particles and two holes. However, the simple power law $E^{(\mathrm{np+nh-1})}$ depends on having unrestricted integrations over momentum direction, which is the case only for a spherical Fermi surface. The more restrictions there are at the upper end of the phase space, the higher the power. The results of Fig. 8 are fairly well fit with the power 5, using the following parametrization,

$$\frac{d^2P}{d\omega\, d\Omega}=4.0\times10^{-10}g(\theta)\frac{(\omega_{\max}-\omega)^5}{\omega_{\max}^{2.5}\omega}\ \mathrm{MeV}^{-1}\ . \tag{5.4}$$

As in the case of proton induced collisional bremsstrahlung, the cross section is obtained by multiplying the differential probability (5.3) by the cross sectional area of the target,

$$\frac{d^2\sigma}{d\omega\, d\Omega}=\pi R^2\frac{d^2P}{d\omega\, d\Omega}\ . \tag{5.5}$$

Since we have neglected the dependence on finite target thickness, this will be a slight overestimate.

We now compare with the measurements of Stevenson *et al.*[4] The cross sections are found to depend on target size as $A^{2/3}$, in agreement with our model. Figure 9 shows the data for ^{14}N + Pb at an incident energy of 40 MeV/N. Our prediction, shown by the solid line, has an ω dependence similar to the data. In the range of energy studied, it could be considered exponential. However, the theory underestimates the magnitude of the cross section by a factor of 3. The laboratory angular distribution is shown in Fig. 9(b) for 30 MeV photons. The solid line shows the predicted yield multiplied by the factor 3. The pronounced forward peaking is well described by the model. This is to be expected if the experimental angular distribution is nearly isotropic in the mid-velocity frame, and the ω dependence is properly reproduced.

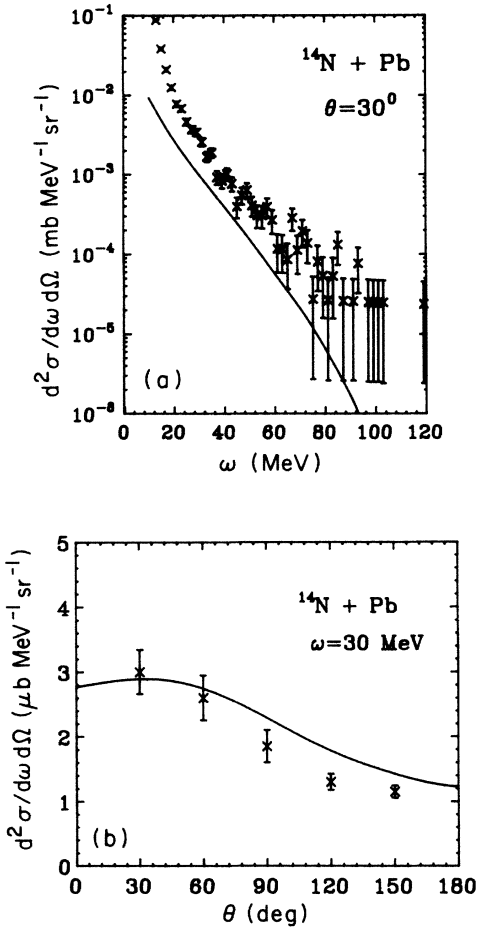

FIG. 9. (a) Energy spectrum of collisional bremstrahlung photons for the reaction ^{14}N + Pb at $E_{\mathrm{lab}}=40$ MeV/N and $\theta=30°$. The data are from Ref. 4. (b) Angular distribution in the lab frame of 30 MeV photons from (a), multiplied by a factor 3. The data are from Ref. 4.

VI. DISCUSSION

We have found that np collisional acceleration is a much more important source of bremsstrahlung than potential well acceleration in certain kinematic regimes of nuclear reactions. The collisional bremsstrahlung will dominate if the kinematics permit photons of much higher energy than the giant dipole, provided that the

photon energies are not at the extreme kinematic limit. This confirms the results of Bauer *et al.*,[8] who found in a TDHF calculation of $^{12}C + ^{12}C$ that the potential well bremsstrahlung was unimportant. The np collisional mechanism describes very well the photons from proton induced reactions, including photon energy dependence, target size dependence, and absolute cross sections. However, the photons produced in heavy ion collisions present more of a problem. Neither potential well acceleration nor first collisions in the double sphere geometry can account for the ultradipole photons in heavy ion collisions.

The weakness of the collisional bremsstrahlung, which is much more difficult to study in TDHF or other realistic treatments of mean field theory, raises a number of questions about our model. First, we must ask whether the double sphere approximation is adequate to describe the phase space distribution of mean field theory. The distribution from TDHF calculations differs from our model somewhat; numerical calculations[15] show a gap in phase space between the two nuclei that never disappears even when the nuclei overlap in coordinate space. If the gap has enough volume to accommodate a particle, the collisional bremsstrahlung could be increased by transitions into the gap. The double sphere model also neglects surface effects. Surface effects are very important in another context: the production of deuterons from high energy heavy ion collisions. The deuteron rate is lower than predicted using bulk arguments, due to the low phase space density in the nuclear surfaces.[20] The surface region, of course, acquires a high weight from the impact parameter averaging in the cross section. However, for our case we do not believe the surface effects are so important. The surface region would be described by smaller spheres, using the Thomas-Fermi approximation. This distribution would have more empty space for collision partners to go to, but there also should not be as much energy available for making ultradipole photons due to the smaller Fermi momentum. In any case, before the direct mechanism can be discarded as the predominant source of high energy photons in heavy ion collisions, further studies are required, especially a more accurate description of the phase space distribution.

Another possibility for explaining the photon yield within conventional nuclear models might be the multiple scattering during the later stages of the collision. This should not be surprising in view of what has been learned about a similar reaction: pion production in low energy heavy ion collisions. That reaction also has small cross sections and should be most sensitive to the early stages of the collision when the energy is most concentrated. However, the cross section is reasonably well described by a statistical treatment.[21,22] For the photon production, the exponential energy spectrum and the nearly isotropic angular distributions in the mid-velocity frame immediately suggest statistical mechanisms. But as we have seen, that is not enough to distinguish the mechanism from the first-collision model. The phase space in the double sphere geometry varies sufficiently rapidly to look exponential over a limited energy regime, and the Pauli effects make the cross section much more isotropic than for free np scattering.

Nifnecker and Bondorf applied a thermal model, parametrizing the number of collisions each participant nucleon makes.[7] To explain the observed yields in 84 MeV/N heavy ion collisions, they require 15—30 collisions per participant nucleon. However, we do not believe there is enough time in the compressed phase of the heavy ion reaction for so many NN collisions to occur. The compressed phase of the collision lasts about 50 fm/c in mean field theory. The collision rate of particles contributing to the ultradipole bremsstrahlung was found to range between 8 and 47 fm/c, allowing an average of three collisions per particle. Clearly, the np collision rate during the middle stages of the nucleus-nucleus interaction needs further study.

Also, Nifenecker and Bondorf assume that the collisions contribute independently to the photon yield. This is only justified if the time between collisions is longer than the inverse frequency of the photon, which is not the case for lower photon energies when the number of collisions is large. This point also deserves further study.

Note added in proof. Our formula for the bremmstrahlung from nucleon-nucleon collisions when applied to the single proton-neutron collision yields a photon cross section which is lower by a factor of 3 to 4 compared to the data of Ref. 1. The meson exchange current is shown to have a negligible contribution for pp bremsstrahlung.[23] However, in np bremsstrahlung the exchange effects are quite important.[24,25] In particular, Brown and Franklin[24] have shown that the inclusion of exchange bremsstrahlung in np collisions increases the photon cross section by a factor ~ 2. Therefore, inclusion of this process may increase the photon cross section in heavy ion collisions. However, it will overestimate the cross section for proton-nucleus-induced reactions. We have learned recently that Neuhauser and Koonin[26] have also calculated photon production cross sections in heavy ion collisions using a fireball model combined with an elementary nucleon-nucleon bremsstrahlung cross section which also accounts for the exchange contributions. They found good agreement with experiment.

ACKNOWLEDGMENTS

We are grateful to W. Benenson and J. Stevenson for conversations and for providing us the data of Ref. 4 prior to publication. We also acknowledge discussions with U. Mosel and W. Bauer on theoretical aspects of photon production. This work was supported by the National Science Foundation under Grant No. PHY 85-19653.

[1] J. Edgington and B. Rose, Nucl. Phys. **89**, 523 (1966).
[2] K. Beard *et al.*, Phys. Rev. C **32**, 1111 (1985).
[3] E. Grosse, quoted in Ref. 7 below, and to be published.
[4] J. Stevenson *et al.*, Phys. Rev. Lett. **57**, 555 (1986).
[5] H. R. Weller *et al.*, Phys. Rev. C **25**, 2921 (1982).
[6] W. Bauer, W. Cassing, U. Mosel, and M. Tohyama, Nucl. Phys. **A456**, 159 (1986).
[7] H. Nifenecker and J. Bondorf, Nucl. Phys. **A442**, 478 (1985).

[8]C. M. Ko, G. Bertsch, and J. Aichelin, Phys. Rev. C **31**, 2324 (1985).
[9]J. Kapusta, Phys. Rev. C **15**, 1580 (1977).
[10]J. D. Bjorken and L. MacLerran, Phys. Rev. D **31**, 63 (1985).
[11]D. Vasak *et al.*, Nucl. Phys. **A428**, 291C (1984).
[12]H. Esbensen and G. Bertsch, Ann. Phys. (N.Y.) **157**, 255 (1984).
[13]In the analytic part, the lack of uniform convergence is treated in the usual way, multiplying the integrand by a convergence factor $e^{-\epsilon|z|}$ and taking the limit $\epsilon \to 0$. Even if the outer contribution is not expressible analytically, it can still be helpful to break up the integral into contributions from the inner and the asymptotic regions; cf. C. M. Vincent and H. T. Fortune, Phys. Rev. C **2**, 782 (1970).
[14]A. Fetter and J. D. Walecka, *Quantum Theory of Many-Particle Systems* (McGraw-Hill, New York, 1979), Eq. (11.62).
[15]H. S. Koehler and H. Flocard, Nucl. Phys. **A323**, 189 (1978).
[16]The total kinetic energy of the system increases during the compressional stage of the collision; cf. Fig. 8 in M. Prakash *et al.*, Nucl. Phys. **A385**, 483 (1982). The kinetic energy increase is not due to particle acceleration entering the overlap region, but rather is due to the reflection of particles from the moving potential well surfaces on the outside.
[17]G. Bertsch, Phys. Rev. C **15**, 713 (1977).
[18]G. Bertsch, Z. Phys. A **289**, 103 (1978).
[19]C. Toepffer and C. Y. Wong, Phys. Rev. C **25**, 1018 (1982).
[20]G. Bertsch, MSU Annual Report, 1980–81, p. 23.
[21]J. Aichelin and G. Bertsch, Phys. Lett. **138B**, 350 (1984).
[22]M. Prakash, P. Braun-Munzinger, and J. Stachel, Phys. Rev. C **33**, 937 (1986).
[23]V. R. Brown, Phys. Rev. **177**, 1498 (1969).
[24]V. R. Brown and J. Franklin, Phys. Rev. C **8**, 1706 (1973).
[25]G. E. Bohannon, L. Heller, and R. H. Thompson, Phys. Rev. C **16**, 284 (1977).
[26]D. Neuhauser and S. E. Koonin, California Institute of Technology Report MAP-80, 1986.